

Current-induced forces and hot-spots in biased nano-junctions

Jing-Tao Lü,^{1,2,3,*} Rasmus B. Christensen,² Jian-Sheng Wang,⁴ Per Hedegård,³ and Mads Brandbyge⁵

¹*School of Physics and Wuhan National High Magnetic Field Center,
Huazhong University of Science and Technology, Wuhan, China*

²*Department of Micro- and Nanotechnology, Technical University of Denmark, Kongens Lyngby, Denmark*

³*Niels Bohr Institute, Nano-Science Center, University of Copenhagen, Copenhagen, Denmark*

⁴*Department of Physics, National University of Singapore, 117551 Singapore, Republic of Singapore*

⁵*Center for Nanostructured Graphene (CNG), Department of Micro- and Nanotechnology,
Technical University of Denmark, Kongens Lyngby, Denmark*

We investigate theoretically the interplay of current-induced forces (CIF), Joule heating, and heat transport inside a current-carrying nano-conductor. We find that the CIF, due to the electron-phonon coherence, can control the spatial heat dissipation in the conductor. This yields a significant asymmetric concentration of excess heating (hot-spot) even for a symmetric conductor. When coupled to the electrode phonons, CIF drive different phonon heat flux into the two electrodes. First-principles calculations on realistic biased nano-junctions illustrate the importance of the effect.

PACS numbers: 85.75.-d, 85.65.+h, 75.75.+a, 73.63.Fg

Introduction– Current-induced forces and Joule heating both originate from the coupling between electrons and phonons[1], one of the most fundamental many-body interactions responsible for a wide range of phenomena in molecular and condensed-matter physics. Their vital role in maintaining the electronic device stability is further promoted at nanoscale. Our understanding of the two closely related effects, especially their interplay in nano- and atomic-conductors is still under development[2–10]. Several forces, present only in the nonequilibrium situation, have been discovered theoretically. Among them are the non-conservative (NC) “wind force”, and the Berry-phase (BP) induced pseudo-magnetic force. Different from the stochastic Joule heating[11–23], the NC and BP forces can generate *deterministic* energy and momentum transfer between the current-carrying electrons and the vibrations in the conductor[2–6]. In carefully designed devices, this effect may be used to drive atomic motors[2, 7]. Meanwhile, it can also impact the stability of the device[3, 24, 25]. To this end, the vibrational/phononic[1] heat transport and heat distribution in the presence of current flow becomes an urgent problem to investigate.

The electrode phonons play an important role as heat sinks for the locally dissipated Joule heat in the conductor[15]. However, the effects on the heat transport of the deterministic CIF, and the momentum transfer from the current has so far not been explored. To address this question, we go beyond the previous treatments[3, 26] considering localized vibrations in the conductor, and include coupling to the phonons in the electrodes[27]. Employing the semi-classical generalized Langevin equation(SGLE)[26, 28–30], we find that, in addition to energy transfer, the CIF also influence how the excess vibrational energy is distributed in the junction and transported to the electrodes. Using first-principles calculations, we demonstrate how *symmetric* current-carrying nano-junctions typically possess a significant *asymmetric* excess heat distribution with heat

accumulation at hot-spots in the junction. At the same time the phonon heat flow to the two electrodes differs. This behavior is governed by the phases of the electron and phonon wavefunctions, and is a result of electron-hole pair symmetry breaking in the electronic structure. It will have important implications, and should be taken into account when considering junction disruption at high bias[24, 31].

Method – In the SGLE approach we adopt the two-probe transport setup, where a “bottleneck” nano-junction (system) is connected to left(*L*) and right(*R*) electrodes. We consider the case where the system region is characterized by a significant current density and deviation from equilibrium. The current-carrying electrons are treated as a nonequilibrium bath, coupling linearly with the system displacement, while the remaining atoms in *L* and *R* form two phonon baths interacting with the system also via a linear coupling. The electron-phonon (e-ph) coupling Hamiltonian can be written as

$$H_{eph} = \sum_{i,j,k} M_{ij}^k (c_i^\dagger c_j + h.c.) \hat{u}_k. \quad (1)$$

Here, $\hat{u}_k = \sqrt{m_k} \hat{x}_k$ is the mass-normalized displacement away from the equilibrium position of the *k*-th atomic degrees of freedom, with m_k the mass, and \hat{x}_k the displacement operator from equilibrium position; $c_i^\dagger (c_j)$ is the electron creation(annihilation) operator for the *i*-(*j*)-th electronic state in the junction. The coupling matrix, M_{ij}^k , is local in real space, non-zero in the system and neglected in *L, R*. We treat the e-ph interaction perturbatively using the electron and phonon states obtained from the Born-Oppenheimer approximation. In order to focus on the effect of CIF, we will ignore the change of Hamiltonian due to the applied voltage.

The SGLE describing the dynamics of the *system atoms* reads,

$$\ddot{U}(t) - F(U(t)) = - \int_{-\infty}^t \Pi^r(t-t') U(t') dt' + f(t), \quad (2)$$

where, U is a vector composed of the mass-normalized displacements of the system, and $F(U(t))$ is the force vector from the potential of the isolated system. We adopt the harmonic approximation, $F(U(t)) = -KU(t)$, with K being the dynamical matrix. The effect of all bath degrees of freedom is hidden in the terms on the right-hand side of the SGLE. Each of them contains separate contributions from the L , R phonons, and the electron bath (e), such that $\Pi^r = \Pi_L^r + \Pi_R^r + \Pi_e^r$ and $f = f_L + f_R + f_e$. The phonon self-energy Π^r describes the time-delayed backaction of the bath on the system due to its motion[3, 26, 28–30]. The second quantum term $f(t)$ is a random force (noise) due to the thermal, or current-induced fluctu-

ation of the bath variables. It is characterized by the correlation matrix $\langle f_\alpha(t) f_\alpha^T(t') \rangle = S_\alpha(t - t')$, with $\alpha = L, R, e$. The two phonon baths (L and R) are assumed to be in thermal equilibrium. Their noise correlation $S_{L/R}$ is related to the $\Pi_{L/R}^r$ through the fluctuation-dissipation theorem, $S_{L/R}(\omega) = (n_B(\omega, T) + \frac{1}{2})\Gamma_{L/R}(\omega)$ with $\Gamma_{L/R}(\omega) = -2\text{Im}\Pi_{L/R}^r(\omega)$, n_B the Bose distribution function (using atomic units, $\hbar = 1$). Due to the electrical current, the electronic bath is not in equilibrium. We define the coupling-weighted electron-hole pair density of states as,[3, 26]

$$\Lambda_{kl}^{\alpha\beta}(\omega) = 2 \sum_{m,n} \langle \psi_m | M^k | \psi_n \rangle \langle \psi_n | M^l | \psi_m \rangle (n_F(\varepsilon_n - \mu_\alpha) - n_F(\varepsilon_m - \mu_\beta)) \delta(\varepsilon_n - \varepsilon_m - \omega), \quad (3)$$

with n_F the Fermi-Dirac distribution, and ψ_n the electron scattering state originating from the n -th channel of electrode α when there is no e-ph interaction. The noise correlation and the backaction term of the electron bath can now be written as,

$$S_e(\omega) = -2\pi \sum_{\alpha\beta} \left[n_B(\omega - (\mu_\alpha - \mu_\beta)) + \frac{1}{2} \right] \Lambda^{\alpha\beta}(\omega), \quad (4)$$

$$\Pi_e^r(\omega) = -\frac{1}{2} (\mathcal{H}\{\Gamma_e(\omega')\}(\omega) + i\Gamma_e(\omega)), \quad (5)$$

$$\Gamma_e(\omega) = -2\pi \sum_{\alpha\beta} \Lambda^{\alpha\beta}(\omega), \quad (6)$$

where $\mathcal{H}\{A\}$ is the Hilbert transform of A .

In the absence of electrical current, the electrons serve as an equilibrium thermal bath, similar to phonons. However, in the presence of current, the term ($\sim \text{Im}\Lambda_{kl}^{RL}$, $k \neq l$) becomes important. It may coherently couple two vibrational modes (kl) inside the system leading to non-zero NC and BP forces. In Eq. (3) we observe that these effects depend on the phase of the electronic wavefunction, and thus the direction of electronic current. Furthermore, the coherent coupling breaks time-reversal symmetry of the noise correlation function, $S_e(t - t') \neq S_e(t' - t)$. Hereafter, we denote these forces by *asymmetric CIF*, and focus on their role for the excess heat distribution and heat transport in the junction.

We will consider the case where all baths are at the same temperature (T), and the electron bath is subject to a nonzero voltage bias ($eV = \mu_L - \mu_R$). To look at the excess heating, we calculate the kinetic energy of atom n from its local displacement correlation function, and

obtain

$$E_n = \sum_{\sigma=x,y,z} \int_0^{+\infty} \omega^2 \text{diag}\{D^r S D^a\}_{n,\sigma}(\omega) \frac{d\omega}{2\pi}. \quad (7)$$

Here D^r (D^a) is the eV -dependent phonon retarded (advanced) Green's function, S is the sum of noise correlation function from all the baths, and $\text{diag}\{A\}_{n,\sigma}$ means the diagonal matrix element of A , corresponding to the n -th atom's σ degrees of freedom.

To study heat transport, we calculate the phonon heat current flowing *into* the bath L as the product of the velocity of the system degrees of freedom, and the force exerted on them by bath L . Applying time average, using the solution of the SGLE, we arrive at a Landauer-like expression (Sec. I, Supplemental Materials (SM))

$$J_L = - \int_{-\infty}^{+\infty} \omega \text{tr} [\Gamma_L(\omega) D^r(\omega) \Lambda^{RL}(\omega) D^a(\omega)] \times (n_B(\omega + eV) - n_B(\omega)) d\omega. \quad (8)$$

Defining the time-reversed phonon spectral function from the left bath $\tilde{\mathcal{A}}_L = D^a \Gamma_L D^r$, and similarly $\mathcal{A}_e = D^r \Lambda^{RL} D^a$, we can write the trace in Eq. (8) in different forms

$$\text{tr}[\Gamma_L D^r \Lambda^{RL} D^a] = \text{tr}[\Gamma_L \mathcal{A}_e] = \text{tr}[\Lambda^{RL} \tilde{\mathcal{A}}_L]. \quad (9)$$

Equations (8) is analogous to the Landauer or non-equilibrium Green's function formula for electron/phonon transport. In our present case the energy current is driven by a non-thermal electron bath with the bias showing up in the Bose distributions and in the coupling function, Λ^{RL} , between phonons and electrical current. The two forms in Eq. (9) emphasize two aspects of the problem. In the first version emphasis is on the coupling, Γ_L of the system vibrations as described

by \mathcal{A}_e , to the phonons of the leads. This is a general formula, which does not explicitly depend on the situation we are considering here, namely that the source of energy is the non-equilibrium electron bath. This aspect is emphasized in the second version. Here the coupling to the electrical current, Λ^{RL} is made explicit, and the complete phonon system including the coupling to leads are in the function $\tilde{\mathcal{A}}_L$. In both forms the asymmetric CIF show up in the different versions of the \mathcal{A} functions. The forces are responsible for the build up of vibrational energy inside the junction, a fact that is present in the two phonon Green's functions D^r and D^a . Apart from this effect the non-equilibrium nature of the electron system shows up in the explicit factor Λ^{RL} in the second version of Eq. (9). This will develop an imaginary part which is not present in equilibrium.

Applying these formulas to a minimal model, in Sec. II of the SM, we have shown analytically that the asymmetric CIF, especially the NC force, generate an asymmetric phonon heat flow and energy distribution, even for a left-right symmetric system.

First Principles calculations— Next we turn to numerical calculation for two concrete nano-junctions. We use SIESTA/TRANSIESTA[32, 33] to calculate the electronic transport, vibrational modes, e-ph coupling employing Ref. 34, and coupling to electrode phonons using Ref. 35, with similar parameters. The effect of current on the stability of gold single atomic junctions has been studied for more than a decade[31, 36]. Here we first consider a symmetric single atom gold chain between two Au(100) electrodes(Fig. 2 inset).[37, 38] We have previously[39] studied the asymmetric forces in this system neglecting the coupling to electrode phonons.

Figure 1 shows the average excess kinetic energy ($\Delta E_n = E_n(eV) - E_n(0)$)[40–45] of atoms along the chain for three different Fermi level E_F . The structure is almost mirror symmetric. When we turn off the asymmetric CIF ($\text{Im}\Lambda^{RL} = 0$) as in previous studies[14, 46], the heating profile follows this symmetry. However, once we include them, the kinetic energy of one side becomes many times higher than that of the other. Meanwhile, the total kinetic energy stored in the system increase significantly. Further analysis shows that both effects are due to the NC force (Fig. 2 in SM).

We now turn to the phonon heat current calculated using Eq. (8), shown in Fig 2 (a). The inclusion of the asymmetric CIF drives much larger heat current into the L bath. Intuitively, this is due to the asymmetric energy accumulation induced by the NC force, e.g., modifying D^r/D^a in Eqs. (8-9). However, there is another contribution at low bias. Ignoring the bias-induced change of $\tilde{\mathcal{A}}_L$, we get opposite heat flow into L and R ($J_L = -J_R$) due to $\text{tr}[\text{Im}\Lambda^{RL}\text{Im}\tilde{\mathcal{A}}_L^0]$. This term drives asymmetric heat flow even in the linear response regime, contributing with a correction to the thermoelectric Peltier coefficient (Sec. I(A) of SM). In the next section, we will show that it can be understood as asymmetric excitation of left- and right-travelling phonon waves.

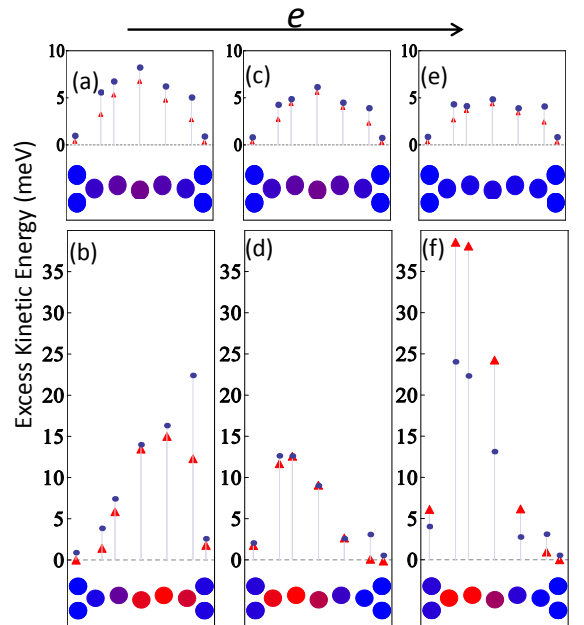


FIG. 1: Excess kinetic energy of each atom in a gold chain (inset of Fig. 2(a)) at $V = 1.0$ V, $T = 300$ K, with (bottom) and without (top) the asymmetric CIF. The total energy difference between the two cases is due to the non-conservative force contribution. The blue dots and the colored plot of each atom are from the full calculation. The asymmetric heating is qualitatively reproduced by only considering electron coupling with vibrational modes (1) and (2) in the inset of Fig. 2 (a), as shown by red triangles. (a)-(b) $E_F = -0.3$ eV, (c)-(d) $E_F = 0$, and (e)-(f) $E_F = 0.2$ eV. The arrow indicates the current direction.

From Fig. 1 (b)-(d) and 2 (b), we see that the position of E_F is controlling the direction and magnitude of the asymmetry. According to the analysis in Sec. IV of SM, this could be due to the phase change of the electronic wavefunction with E_F . Thus we expect that the direction of electron flow is essential in the description of the atomic dynamics in the junction, as indicated in recent experiments[8].

The second system we consider is an armchair graphene nanoribbon (a-GNR) with partial hydrogen passivation, shown in Fig. 3 (a). This example is inspired by experiments showing current-induced edge-reconstructions in graphene[47] where the physical mechanism was attributed to Joule heating[48]. In Fig. 3 (a), the four pairs of unpassivated carbon dimers give rise to localized high-frequency vibrations interacting strongly with electrical current. Consequently, the excess energy is mainly stored in the dimers and nearby atoms (Fig. 3 (b),(d)), consistent with the experimental findings in Ref. 47. Including the asymmetric CIF leads to symmetry breaking of the heating profile along the current direction. Contrary to experiments on the gold chain E_F may in this case be tuned by gating. We predict the resulting hot-spot to move from “down-stream” to “up-

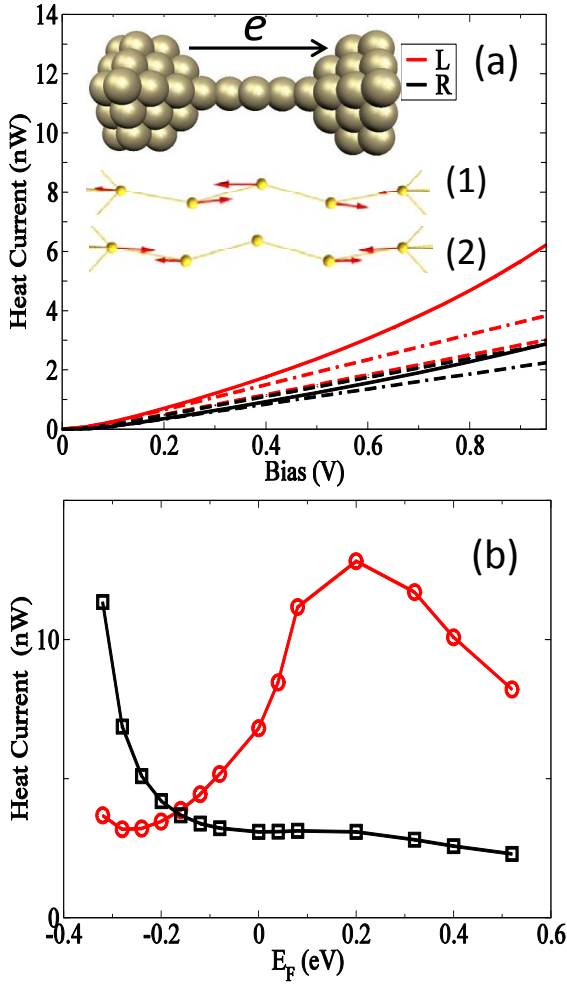


FIG. 2: (a) Bias dependence of the phonon heat current, going into the left and right phonon baths. Solid lines include the asymmetric CIF ($\sim \text{Im}\Lambda^{RL}$), dashed lines do not, and the dash-dotted lines ignore the change of phonon spectral (D^r/D^a) due to NC and BP forces. In the inset, we show the two vibrational modes that couple most strongly with the electrical current, with vibrational energy at (1) 19 and (2) 18 meV. (b) Phonon heat current going into the left (red, circle) and right (black, square) baths at $V = 1\text{ V}$, for different Fermi levels to illustrate the importance of the phase of the electron wavefunctions.

stream" w.r.t. the electron current when tuning from $E_F = 1.4\text{ eV}$ to $E_F = -1.0\text{ eV}$ (Fig. 3 (c),(e), and Fig. 3 in SM). Thus, our calculation further suggests that which part of the edge bonds break first may be controlled by gating.

The dependence of the hot-spot on E_F can be understood as follows (Sec. III of SM). For a mirror-symmetric system with electron-hole symmetry, the asymmetric heating and heat flow is absent. When E_F crosses the electron-hole symmetric point, the dominant current-carriers contributing to inelastic transport change from electrons to holes, or vice versa. Thus, the hot-spot

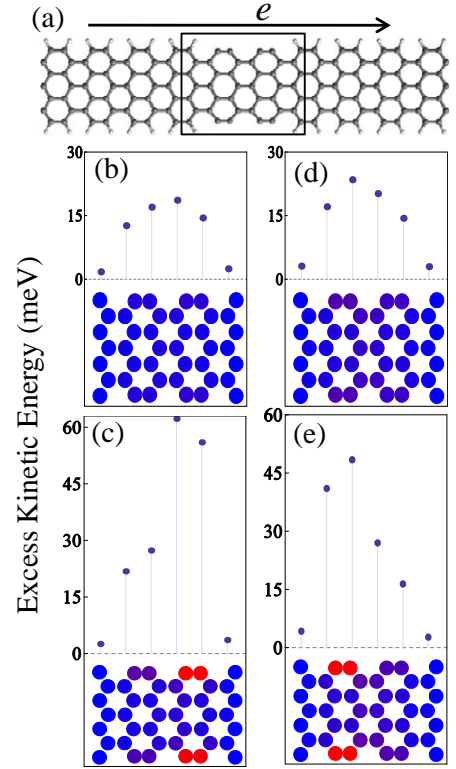


FIG. 3: (a) Structure of a partially passivated armchair graphene ribbon considered. The two sides of the ribbon is hydrogen passivated except in the device region, enclosed by the solid lines. (b)-(c) The excess kinetic energy of each atom without and with the asymmetric CIF, at $V = 0.4\text{ V}$, $T = 300\text{ K}$, $E_F = 1.4\text{ eV}$. The dots show the average over atoms belonging to each zigzag column. (d)-(e) Same with (b)-(c) with $E_F = -1.0\text{ eV}$.

moves from one side to the other. Interestingly enough, similar effect in micrometer scale has been observed experimentally in graphene transistors[49, 50] and electrodes of molecular junctions[23]. Here we show that it is equally important at atomic scale, and related to the asymmetric CIF.

Scattering analysis – The asymmetric heating and phonon heat flow at low bias can be qualitatively understood from the momentum transfer between electrons and phonons. To show this, we consider a simple 1D model with a local e-ph interaction which involve the displacement of the n - and $n + 1$ -th atoms (junction) (Sec. IV of SM),

$$H_{eph} = \sum_{j \in \{n, n+1\}} -m\hat{u}_j(c_j^\dagger c_{j+1} - c_j^\dagger c_{j-1} + h.c.). \quad (10)$$

For $eV > 0$, the important process is the inelastic electronic transition from the filled, left scattering states with momentum k_L to the empty, right states with k_R . It is straightforward to show that the emission probability of a right-travelling phonon with momentum q is different from that of a left-travelling mode, $-q$, due to the differ-

ence in matrix elements for the processes,

$$\Delta M_{LR} = |M_{LR}^q|^2 - |M_{LR}^{-q}|^2 \sim \sin(q) \sin(k_L - k_R). \quad (11)$$

Consequently, the left- and right-travelling steady state phonon populations become different, resulting in asymmetric heat flow.

In conclusion, we have presented a theory showing that CIF in nano-junctions lead to asymmetric distributions and transport of the excess heat. We derived a Landauer-like formula for the excess heat transport. Employing first-principles calculations, we demonstrate that the size

of the asymmetry can be crucial for current-induced processes at the atomic scale.

We thank T. N. Todorov, D. Dundas, and T. Markussen for discussions and the Danish Center for Scientific Computing (DCSC) for computer resources. This work is supported by the Lundbeck Foundation (R49-A5454), National Natural Science Foundation of China (Grants No. 11304107, 61371015), and the Fundamental Research Funds for the Central Universities (HUST:2013TS032).

* Electronic address: jtl@hust.edu.cn

- [1] We use phonons and vibrations interchangeably, although, strictly speaking, phonons are defined only in systems with translational invariance.
- [2] D. Dundas, E. J. McEniry, and T. N. Todorov, *Nature Nanotech.* **4**, 99 (2009).
- [3] J. T. Lü, M. Brandbyge, and P. Hedegård, *Nano Lett.* **10**, 1657 (2010).
- [4] N. Bode, S. V. Kusminskiy, R. Egger, and F. von Oppen, *Phys. Rev. Lett.* **107**, 036804 (2011).
- [5] T. N. Todorov, D. Dundas, A. T. Paxton, and A. P. Horsfield, *Beilstein Journal of Nanotechnology* **2**, 727 (2011).
- [6] I. A. Pshenichnyuk and M. Čížek, *Phys. Rev. B* **83**, 165446 (2011).
- [7] R. Bustos-Marín, G. Refael, and F. von Oppen, *Phys. Rev. Lett.* **111**, 060802 (2013).
- [8] C. Schirm, M. Matt, F. Pauly, J. C. Cuevas, P. Nielaba, and E. Scheer, *Nature Nanotech.* **8**, 645 (2013).
- [9] P. J. Wheeler, R. Chen, and D. Natelson, *Phys. Rev. B* **87**, 155411 (2013).
- [10] B. Cunningham, T. N. Todorov, and D. Dundas, *Phys. Rev. B* **90**, 115430 (2014).
- [11] N. J. Tao, *Nature Nanotech.* **1**, 173 (2006).
- [12] M. Galperin, M. A. Ratner, and A. Nitzan, *J. Phys.:Condens. Matter* **19**, 103201 (2007).
- [13] M. Galperin, M. A. Ratner, A. Nitzan, and A. Troisi, *Science* **319**, 1056 (2008).
- [14] Z. Huang, F. Chen, R. D'Agosta, P. A. Bennett, M. Di Ventra, and N. Tao, *Nature Nanotech.* **2**, 698 (2007).
- [15] M. Tsutsui, M. Taniguchi, and T. Kawai, *Nano Lett.* **8**, 3293 (2008).
- [16] Y. Asai, *Phys. Rev. B* **78**, 045434 (2008).
- [17] R. H. M. Smit, Y. Noat, C. Untiedt, N. D. Lang, M. C. van Hemert, and J. M. van Ruitenbeek, *Nature* **419**, 906 (2002).
- [18] W. Y. Wang, T. Lee, I. Kretschmar, and M. A. Reed, *Nano Lett.* **4**, 643 (2004).
- [19] J. G. Kushmerick, J. Lazorcik, C. H. Patterson, R. Shashidhar, D. S. Seferos, and G. C. Bazan, *Nano Lett.* **4**, 639 (2004).
- [20] Z. Ioffe, T. Shamai, A. Ophir, G. Noy, I. Yutsis, K. Kfir, O. Cheshnovsky, and Y. Selzer, *Nature Nanotech.* **3**, 727 (2008).
- [21] D. R. Ward, D. A. Corley, J. M. Tour, and D. Natelson, *Nature Nanotech.* **6**, 33 (2011).
- [22] K. Kaasbjerg, T. c. v. Novotný, and A. Nitzan, *Phys. Rev. B* **88**, 201405 (2013).
- [23] W. Lee, K. Kim, W. Jeong, L. A. Zotti, F. Pauly, J. C. Cuevas, and P. Reddy, *Nature* **498**, 209 (2013).
- [24] R. H. M. Smit, C. Untiedt, and J. M. van Ruitenbeek, *Nanotechnology* **15**, S472 (2004).
- [25] G. Schulze, K. J. Franke, A. Gagliardi, G. Romano, C. S. Lin, A. L. Rosa, T. A. Niehaus, T. Frauenheim, A. Di Carlo, A. Pecchia, et al., *Phys. Rev. Lett.* **100**, 136801 (2008).
- [26] J.-T. Lü, M. Brandbyge, P. Hedegård, T. N. Todorov, and D. Dundas, *Phys. Rev. B* **85**, 245444 (2012).
- [27] J.-S. Wang, *Phys. Rev. Lett.* **99**, 160601 (2007).
- [28] R. P. Feynman and F. L. Vernon, *Ann. Phys.* **24**, 118 (1963).
- [29] A. Caldeira and A. Leggett, *Physica A* **121**, 587 (1983).
- [30] A. Schmid, *J. Low Temp. Phys.* **49**, 609 (1982).
- [31] Y. Oshima and Y. Kurui, *Phys. Rev. B* **87**, 081404 (2013).
- [32] J. Soler, E. Artacho, J. Gale, A. Garcia, J. Junquera, P. Ordejon, and D. Sanchez-Portal, *J. Phys.:Condens. Matter* **14**, 2745 (2002).
- [33] A. Brandbyge, J. L. Mozos, P. Ordejon, J. Taylor, and K. Stokbro, *Phys. Rev. B* **65**, 165401 (2002).
- [34] T. Frederiksen, M. Paulsson, M. Brandbyge, and A.-P. Jauho, *Phys. Rev. B* **75**, 205413 (2007).
- [35] M. Engelund, M. Brandbyge, and A. P. Jauho, *Phys. Rev. B* **80**, 045427 (pages 11) (2009).
- [36] H. Yasuda and A. Sakai, *Phys. Rev. B* **56**, 1069 (1997).
- [37] H. Ohnishi, Y. Kondo, and K. Takayanagi, *Nature* **395**, 780 (1998).
- [38] A. I. Yanson, G. R. Bollinger, H. E. van den Brom, N. Agraït, and J. M. van Ruitenbeek, *Nature* **395**, 783 (1998).
- [39] J. T. Lü, P. Hedegård, and M. Brandbyge, *Phys. Rev. Lett.* **107**, 046801 (2011).
- [40] Y. Dubi and M. Di Ventra, *Phys. Rev. B* **79**, 115415 (2009).
- [41] Y. Dubi and M. Di Ventra, *Phys. Rev. E* **79**, 042101 (2009).
- [42] P. A. Jacquet, *J Stat Phys* **134**, 709 (2009).
- [43] P. A. Jacquet and C.-A. Pillet, *Phys. Rev. B* **85**, 125120 (2012).
- [44] J. P. Bergfield, S. M. Story, R. C. Stafford, and C. A. Stafford, *ACS Nano* **7**, 4429 (2013).
- [45] Another way of quantifying the heating is to use the local temperature defined in some way. We tried to use the method in Refs. [40-44]. The result is shown in Fig. 3 of

the SM. The overall heating profile agrees with Fig. 1.

- [46] T. Frederiksen, M. Brandbyge, N. Lorente, and A.-P. Jauho, Phys. Rev. Lett. **93**, 256601 (2004).
- [47] X. Jia, M. Hofmann, V. Meunier, B. G. Sumpter, J. Campos-Delgado, J. M. Romo-Herrera, H. Son, Y.-P. Hsieh, A. Reina, J. Kong, et al., Science **323**, 1701 (2009).
- [48] M. Engelund, J. A. Fürst, A. P. Jauho, and M. Brandbyge, Phys. Rev. Lett. **104**, 036807 (2010).
- [49] M. Freitag, H.-Y. Chiu, M. Steiner, V. Perebeinos, and P. Avouris, Nature Nanotechnology **5**, 497 (2010), 1004.0369.
- [50] M.-H. Bae, Z.-Y. Ong, D. Estrada, and E. Pop, Nano Letters **10**, 4787 (2010), 1004.0287.

SUPPLEMENTAL MATERIALS

I. DERIVATION OF THE PHONON HEAT CURRENT EQ. (8)

We start from the semi-classical generalized Langevin equation (SGLE) (Eq. (2) in the main text). To study the energy transport, we look at the energy increase of the system per unit time

$$\begin{aligned}\dot{E}_S(t) &= \frac{d}{dt} \left(\frac{1}{2} \dot{U}^T \dot{U} + \frac{1}{2} U^T K U \right) \\ &= -\dot{U}^T \left(\sum_{\alpha} \int_{-\infty}^t \Pi_{\alpha}^r(t-t') U(t') dt' - f_{\alpha}(t) \right), \quad \alpha = L, R, e.\end{aligned}\quad (12)$$

Note that the system includes only the atomic degrees of freedom. We can define the energy current flowing *into* the bath α from the system

$$J_{\alpha}(t) \equiv \dot{U}^T \left(\int_{-\infty}^t \Pi_{\alpha}^r(t-t') U(t') dt' - f_{\alpha}(t) \right). \quad (13)$$

At steady state we have

$$-\dot{E}_s \equiv J_e + J_L + J_R \equiv J_e + J_{ph} = 0. \quad (14)$$

We can write the expression for the average energy current in the frequency domain,

$$\begin{aligned}J_{\alpha} &\equiv \lim_{T \rightarrow +\infty} \frac{1}{T} \int_0^T \left\langle \dot{U}^T(t) \left(\int_{-\infty}^t \Pi_{\alpha}^r(t-t') U(t') dt' - f_{\alpha}(t) \right) \right\rangle dt \\ &= \lim_{T \rightarrow +\infty} \frac{1}{T} \int \frac{d\omega}{2\pi} \langle \dot{U}^{\dagger}(\omega) (\Pi_{\alpha}^r(\omega) U(\omega) - f_{\alpha}(\omega)) \rangle\end{aligned}\quad (15)$$

Now we use the solution of the Langevin equation

$$U(\omega) = -D^r(\omega) f(\omega), \quad (16)$$

$$D^r(\omega) = [\omega^2 - K - \Pi^r(\omega)]^{-1}, \quad (17)$$

$$\Pi^r(\omega) = \Pi_L(\omega) + \Pi_R(\omega) + \Pi_e(\omega), \quad (18)$$

and the noise correlation function

$$\langle f_{\alpha}(\omega) f_{\alpha}(\omega') \rangle = \delta(\omega + \omega') S_{\alpha}(\omega), \quad (19)$$

$$S(\omega) = S_L(\omega) + S_R(\omega) + S_e(\omega), \quad (20)$$

to get ($\hbar = 1$)

$$J_{\alpha} = i \int_{-\infty}^{+\infty} \frac{d\omega}{2\pi} \omega \text{Tr} [\Pi_{\alpha}^r(\omega) D^r(\omega) S(\omega) D^a(\omega) + S_{\alpha}(\omega) D^a(\omega)] \quad (21)$$

$$= i \int_0^{+\infty} \frac{d\omega}{2\pi} \omega \text{Tr} [\Pi_{\alpha}^r(\omega) D^r(\omega) S(\omega) D^a(\omega) + S_{\alpha}(\omega) D^a(\omega) \quad (22)$$

$$- \Pi_{\alpha}^r(-\omega) D^r(-\omega) S(-\omega) D^a(-\omega) - S_{\alpha}(-\omega) D^a(-\omega)]. \quad (23)$$

The two phonon baths (L and R) are assumed to be in thermal equilibrium. Their noise correlation $S_{L/R}$ is related to the $\Pi_{L/R}^r$ through the fluctuation-dissipation theorem, $S_{L/R}(\omega) = (n_B(\omega, T) + \frac{1}{2}) \Gamma_{L/R}(\omega)$ with $\Gamma_{L/R}(\omega) = -2\text{Im}\Pi_{L/R}^r(\omega)$, n_B the Bose distribution function (using atomic units, $\hbar = 1$). The noise correlation of the electron bath is given by Eqs. (3)-(4) in the main text. Using the following properties

$$(D^r)^{\dagger}(\omega) = D^a(\omega), (\Pi^r)^{\dagger}(\omega) = \Pi^a(\omega), \Gamma(\omega) = i(\Pi^r(\omega) - \Pi^a(\omega)), \quad (24)$$

$$S^{\dagger}(\omega) = S(\omega), S(-\omega) = S^*(\omega), D^r(-\omega) = (D^r)^*(\omega), D^a(-\omega) = (D^a)^*(\omega), \quad (25)$$

and taking transpose of Eq. (23), we get a compact form

$$J_\alpha = \int_0^{+\infty} \frac{d\omega}{2\pi} \omega \text{Tr} [\Gamma_\alpha(\omega) D^r(\omega) S_{\bar{\alpha}}(\omega) D^a(\omega) - S_\alpha(\omega) D^r(\omega) \Gamma_{\bar{\alpha}}(\omega) D^a(\omega)]. \quad (26)$$

This result has a clear physical meaning. Here, Γ_α characterizes coupling of the α bath to the system, and $S_{\bar{\alpha}}$ represents the energy source from all other baths. The first term in the trace represents energy flow into bath α from other baths; while the second one represents the opposite process.

A. Current-induced phonon heat transport

Now suppose all the baths are at the same temperature (T), but the electron bath is subject to a nonzero bias (eV). The energy current injecting into the phonon bath (L) is

$$J_L = \int_0^{+\infty} \frac{d\omega}{2\pi} \omega \text{Tr} [\Gamma_L(\omega) D^r(\omega) S_{\bar{\alpha}}(\omega) D^a(\omega) - S_L(\omega) D^r(\omega) \Gamma_{\bar{\alpha}}(\omega) D^a(\omega)] \quad (27)$$

$$= \int_0^{+\infty} \frac{d\omega}{2\pi} \omega \text{Tr} [\Gamma_L(\omega) D^r(\omega) S_e(\omega) D^a(\omega) - S_L(\omega) D^r(\omega) \Gamma_e(\omega) D^a(\omega)]. \quad (28)$$

To go from Eq. (27) to (28), we notice that the energy flow from L to R is the same as that from R to L , since they are at the same temperature. Thus, the only energy source is the electron bath. Using Eqs. (3-6) in the main text, the heat current now reads

$$J_L = - \sum_{\alpha \neq \beta} \int_0^{+\infty} d\omega \omega \text{Tr} [\Lambda^{\alpha\beta}(\omega) D^a(\omega) \Gamma_L(\omega) D^r(\omega)] (n_B(\omega - (\mu_\alpha - \mu_\beta)) - n_B(\omega)) \quad (29)$$

$$= - \int_0^{+\infty} d\omega \omega \text{Tr} [\Lambda^{RL}(\omega) D^a(\omega) \Gamma_L(\omega) D^r(\omega)] (n_B(\omega + eV) - n_B(\omega)). \quad (30)$$

Define the time-reversed phonon spectral function $\tilde{\mathcal{A}}_L(\omega) = D^a(\omega) \Gamma_L(\omega) D^r(\omega)$, we can write it in other equivalent forms

$$J_L = - \int_{-\infty}^{+\infty} d\omega \omega \text{Tr} [\Lambda^{LR}(\omega) \tilde{\mathcal{A}}_L(\omega)] (n_B(\omega - eV) - n_B(\omega)) \quad (31)$$

$$= - \int_{-\infty}^{+\infty} d\omega \omega \text{Tr} [\Lambda^{RL}(\omega) \tilde{\mathcal{A}}_L(\omega)] (n_B(\omega + eV) - n_B(\omega)). \quad (32)$$

Similar equation holds for J_R

$$J_R = - \int_{-\infty}^{+\infty} d\omega \omega \text{Tr} [\Lambda^{RL}(\omega) \tilde{\mathcal{A}}_R(\omega)] (n_B(\omega + eV) - n_B(\omega)) \quad (33)$$

$$= - \int_{-\infty}^{+\infty} d\omega \omega \text{Tr} [\Lambda^{LR}(\omega) \tilde{\mathcal{A}}_R(\omega)] (n_B(\omega - eV) - n_B(\omega)). \quad (34)$$

Let's look at the low bias situation. We ignore the change of $\tilde{\mathcal{A}}_{L/R}$, and replace it with $\tilde{\mathcal{A}}_L^0$, the counterpart of $\tilde{\mathcal{A}}_L$ without coupling to electrons. The asymmetric current-induced forces ($\sim \text{Im}\Lambda^{RL}$) drive a heat current

$$J_{L,p}^0 = \frac{1}{2} \int_{-\infty}^{+\infty} d\omega \omega \text{Tr} [\text{Im}\Lambda^{RL}(\omega) \text{Im}\tilde{\mathcal{A}}_L^0(\omega)] \left(\coth\left(\frac{\omega + eV}{2k_B T}\right) - \coth\left(\frac{\omega}{2k_B T}\right) \right), \quad (35)$$

The expression for $J_{R,p}^0$ is obtained by replacing $\tilde{\mathcal{A}}_L^0$ with $\tilde{\mathcal{A}}_R^0$. From $\text{Im}\tilde{\mathcal{A}}_L^0 + \text{Im}\tilde{\mathcal{A}}_R^0 = 0$, we get $J_{L,p}^0 = -J_{R,p}^0$. That is, the heat flowing into bath L and R is opposite. This makes $J_L \neq J_R$, even for a symmetric structure. Furthermore, in the linear response regime, considering thermoelectric transport, from Eq. (35) we get a correction to the Peltier coefficient due to electron-phonon interaction: The applied bias drives a phonon heat current from one phonon bath to the other.

From the derivation of Eq. (35), and (21), we observe that, the first term with $\omega \coth((\omega + eV)/(2k_B T))$ in $J_{L,p}^0$ is contributed by the fluctuating force in the SGLE, while the second term with $\omega \coth(\omega/(2k_B T))$ is from the

deterministic NC force. If the bias $|eV|$ is much higher than the phonon frequency, the contribution from NC force dominates. This can be seen from the symmetry of the functions, as follows: for high enough bias, $\omega \coth((\omega + eV)/(2k_B T))$ is close to be odd in ω , e.g., ignoring ω in the coth function. But $\omega \coth(\omega/(2k_B T))$ is even in ω . Meanwhile, the trace in Eq. (35) can be approximated by an even function for small ω . Thus, the contribution of the NC force dominates. The above analysis based on Eq. (35) is correct to the 2nd order in M . Going beyond the 2nd order, we notice that in Eqs. (31-34), the deterministic NC and BP force modifies the phonon spectral function $\tilde{\mathcal{A}}_{L/R}$, while the fluctuating force has no effect on it. Altogether, we conclude that, the asymmetric noise has a negligible contribution to the asymmetric heat flow.

II. MINIMAL MODEL

We now consider a minimal model with two atomic vibrations. In addition to electrons, they couple symmetrically to the left and right phonon bath, respectively. This gives rise to lifetime broadening of γ_e and γ_{ph} , respectively. The phonon Green's function is written as

$$D^r(\omega) = \frac{1}{N} \begin{pmatrix} \Omega & -\omega_1^2 - a - ib\omega \\ -\omega_1^2 + a + ib\omega & \Omega \end{pmatrix}. \quad (36)$$

Here, $\Omega = \omega^2 - \omega_0^2 + i\gamma_t\omega$, $\gamma_t = \gamma_e + \gamma_{ph}$, $N = \Omega^2 - (\omega_1^2 + a + ib\omega)(\omega_1^2 - a - ib\omega)$, a and b are due to NC and BP forces, respectively. Finally, ω_0 is the atomic vibration frequency, and ω_1 characterizes the coupling between the two sites. We have ignored a term $\sim -i\gamma'_e\omega$ in the off-diagonals of $D^r(\omega)$. The advanced Green's function is $D^a = (D^r)^\dagger$. We also have

$$\tilde{\Pi}_L(\omega) = -2i\gamma_{ph}\omega \begin{pmatrix} 1 & 0 \\ 0 & 0 \end{pmatrix}. \quad (37)$$

From these, we get the time-reversed phonon left spectral function

$$\tilde{\mathcal{A}}_L(\omega) = \frac{2\omega\gamma_{ph}}{|N|^2} \begin{pmatrix} |\Omega|^2 & -(a + ib\omega + \omega_1^2)\Omega^* \\ -(a - ib\omega + \omega_1^2)\Omega & \omega_1^4 + a^2 + b^2\omega^2 + 2a\omega_1^2 \end{pmatrix}, \quad (38)$$

A. Heat current

To calculate the heat current, we assume

$$\Lambda^{\alpha\beta}(\omega) \approx -2(\omega - (\mu_\alpha - \mu_\beta)) \begin{pmatrix} \lambda_1^{\alpha\beta} & \lambda_2^{\alpha\beta} + i\lambda_3^{\alpha\beta} \\ \lambda_2^{\alpha\beta} - i\lambda_3^{\alpha\beta} & \lambda_1^{\alpha\beta} \end{pmatrix}. \quad (39)$$

This means we ignore the energy dependence of the electronic properties within the bias window. We can now evaluate the trace in Eq. (32),

$$\text{Tr} [\text{Im}\Lambda^{RL}\text{Im}\tilde{\mathcal{A}}_L] = -\frac{8}{|N|^2}\omega^2(\omega + eV)\gamma_{ph} \left[\frac{1}{\omega_c}eV\lambda_3^2(\omega_0^2 - \omega^2) + eV\lambda_3^2\gamma_t \underbrace{-\lambda_3\omega_1^2\gamma_t}_{\text{curly bracket}} \right], \quad (40)$$

$$\begin{aligned} \text{Tr} [\text{Re}\Lambda^{RL}\text{Re}\tilde{\mathcal{A}}_L] &= -\frac{4}{|N|^2}\omega(\omega + eV)\gamma_{ph} \left[|\Omega|^2\lambda_1 + \lambda_1 \left(\omega_1^4 + eV^2\lambda_3^2 \left(1 + \frac{\omega^2}{\omega_c^2} \right) \right) \right. \\ &\quad \left. - 2\lambda_2\omega_1^2(\omega^2 - \omega_0^2) + 2eV\lambda_3 \underbrace{\left[\lambda_2 \left(\frac{\omega^2}{\omega_c}\gamma_t + (\omega^2 - \omega_0^2) \right) - \lambda_1\omega_1^2 \right]}_{\text{curly bracket}} \right]. \end{aligned} \quad (41)$$

We have dropped the RL superscript in λ s for notational simplicity, and used $a = -eV\lambda_3^{RL}$, $b = a/\omega_c$. Here ω_c is on the order of the electron bandwidth. Substituting back into Eq. (32), we find that those terms in the curly brackets of Eqs. (40) and (41), due to the asymmetric current-induced forces ($\sim \lambda_3$), induce asymmetric heat flow (odd in eV) to the left and right phonon bath.

B. Average kinetic energy

We now calculate the average kinetic energy difference between the two atomic sites. If we take a general noise correlation for the electronic bath

$$S_e(\omega, eV) = \sum_{\alpha, \beta = \{L, R\}} g^{\alpha\beta}(\omega) \begin{pmatrix} \lambda_1^{\alpha\beta} & \lambda_2^{\alpha\beta} + i\lambda_3^{\alpha\beta} \\ \lambda_2^{\alpha\beta} - i\lambda_3^{\alpha\beta} & \lambda_1^{\alpha\beta} \end{pmatrix}, \quad (42)$$

with

$$g^{\alpha\beta}(\omega) = 2\pi(\omega - (\mu_\alpha - \mu_\beta)) \coth\left(\frac{\omega - (\mu_\alpha - \mu_\beta)}{2k_B T}\right). \quad (43)$$

Using Eq. (6) in the main text, we get

$$\Delta E^e = \sum_{\alpha, \beta = L, R} \int \frac{\omega^2 g^{\alpha\beta}(\omega)}{|N|^2} \left[\lambda_2^{\alpha\beta} (a(\omega^2 - \omega_0^2) + b\omega^2 \gamma_t) - a\lambda_1^{\alpha\beta} \omega_1^2 - \lambda_3^{\alpha\beta} \gamma_t \omega \omega_1^2 \right] \frac{d\omega}{2\pi}. \quad (44)$$

We look at the nonequilibrium contribution first $S_e^{non}(\omega) = S_e(\omega, eV) - S_e(\omega, 0)$. For $eV \gg \omega_0$, similar arguments to Sec. IA show that the main contribution comes from the real part of the two terms with $\alpha \neq \beta$, and the asymmetric noise is negligible,

$$S_e^{non}(\omega) \sim 2\pi|eV| \begin{pmatrix} \lambda_1^{RL} & \lambda_2^{RL} \\ \lambda_2^{RL} & \lambda_1^{RL} \end{pmatrix}, \quad eV \gg \omega_0. \quad (45)$$

Consequently, we get

$$\Delta E^{non} \approx \int \frac{4\pi\omega^2 eV \lambda_3^{RL} |eV|}{|N|^2} \left[\lambda_2^{RL} \left(\omega^2 - \omega_0^2 + \frac{\omega^2 \gamma_t}{\omega_c} \right) - \lambda_1^{RL} \omega_1^2 \right] \frac{d\omega}{2\pi}. \quad (46)$$

The BP force contribution is negligible if ω_c is the largest energy scale of the problem. If we further ignore λ_2^{RL} to be consistent with Eq. (36), we get

$$\Delta E^{non} \approx -4\pi eV |eV| \lambda_3^{RL} \lambda_1^{RL} \omega_1^2 \int \frac{\omega^2}{|N|^2} \frac{d\omega}{2\pi}. \quad (47)$$

For the equilibrium part, including contribution from phonon baths, we get

$$\Delta E^{equ} \approx -eV \lambda_3^{RL} (\gamma_{ph} + \gamma_e) \omega_1^2 \int \frac{\omega^3}{|N|^2} \coth\left(\frac{\omega}{2k_B T}\right) \frac{d\omega}{2\pi}, \quad (48)$$

The total difference $\Delta E^e = \Delta E^{non} + \Delta E^{equ}$. We see that $\Delta E^e = 0$ if $\lambda_3^{RL} = 0$. Thus, the asymmetric current-induced forces generate asymmetric energy distribution, with the NC force contributes predominantly. The asymmetry is enhanced by coupling to phonon baths (γ_{ph} in Eq. (48)).

III. ELECTRON-HOLE SYMMETRY

Assuming symmetrical voltage drop across the conductor, we define the zero energy as the equilibrium Fermi level. The left and right chemical potential are at $eV/2$ and $-eV/2$, respectively. The Λ -function now reads

$$\Lambda_{kl}^{\alpha\beta}(\omega, eV) = 2 \sum_{m,n} \langle \psi_m | M^k | \psi_n \rangle \langle \psi_n | M^l | \psi_m \rangle [n_F(\varepsilon_n - s_\alpha eV/2) - n_F(\varepsilon_m - s_\beta eV/2)] \delta(\varepsilon_n - \varepsilon_m - \omega), \quad (49)$$

where we have written explicitly its eV dependence, and $s_L = 1$, $s_R = -1$. It has the following properties:

$$\Lambda_{kl}^{\alpha\beta}(\omega, eV) = \Lambda_{lk}^{\alpha\beta*}(\omega, eV), \quad \Lambda_{kl}^{\alpha\beta}(\omega, eV) = -\Lambda_{lk}^{\beta\alpha}(-\omega, eV). \quad (50)$$

For the convenience of further analysis, we now use

$$A_\alpha(\varepsilon) = 2\pi \sum_n |\psi_n\rangle \delta(\varepsilon - \varepsilon_n) \langle \psi_n|, \quad (51)$$

to write it as

$$\Lambda_{kl}^{\alpha\beta}(\omega, eV) = 2 \int \frac{d\varepsilon}{2\pi} \int \frac{d\varepsilon'}{2\pi} \text{Tr} [M^k A_\alpha(\varepsilon) M^l A_\beta(\varepsilon')] [n_F(\varepsilon - s_\alpha eV/2) - n_F(\varepsilon' - s_\beta eV/2)] \delta(\varepsilon - \varepsilon' - \omega), \quad (52)$$

Note that the spectral function $A_\alpha(\varepsilon)$ is Hermitian. If we use a real-space basis set, it is a complex matrix. We define the system has electron-hole symmetry if

$$\text{Re}A_\alpha(\varepsilon) = \text{Re}A_\alpha(-\varepsilon), \quad \text{or} \quad A_\alpha(\varepsilon) = A_\alpha^*(-\varepsilon), \quad (53)$$

The two conditions are equivalent since $\text{Re}A_\alpha(\varepsilon)$ is related to $\text{Im}A_\alpha(\varepsilon)$ by Hilbert transform, which changes their symmetry with respect to ε . Using Eq. (53) in (52), together with Eq. (50), we find that

$$\Lambda^{LR}(\omega, eV) = \Lambda^{RL}(\omega, -eV). \quad (54)$$

Here, we have further assumed that the electron-phonon interaction matrix is real. This is a reasonable assumption, if we ignore the bias-dependence of the electronic Hamiltonian, and consider Cartesian phonon index, without external magnetic field. Substituting it into Eqs. (31-32) and (33-34), we find that

$$J_\alpha(eV) = J_\alpha(-eV), \quad \alpha = L, R. \quad (55)$$

We reach the conclusion that the heat flow into L and R are the same if the system has electron-hole symmetry and there is a symmetrical voltage drop across the conductor.

IV. SCATTERING ANALYSIS

The asymmetric heating and heat flow at low bias can be qualitatively understood as momentum transfer between electrons and phonons. To show this, we consider a simple one-dimensional (1D) model. The electronic subsystem is described by a nearest neighbour tight-binding Hamiltonian, and the phonon subsystem by a harmonic oscillator model. To simplify the analysis, we assume that the tight-binding hopping parameter and the spring constant between all the nearest sites are the same. But the analysis can be easily extended to more general case, where our conclusion in this section still holds. The electron and phonon states are described by scattering waves originating from L and R . We introduce a local e-ph interaction on two atomic sites n and $n+1$ (junction), that is, the displacement of the n - and $n+1$ -th atoms modifies the electronic hopping elements nearby linearly, e.g., for phonon mode q ,

$$M^q \sim \begin{pmatrix} 0 & 1 & 0 & 0 \\ 1 & 0 & -1 + e^{iq} & 0 \\ 0 & -1 + e^{iq} & 0 & -e^{iq} \\ 0 & 0 & -e^{iq} & 0 \end{pmatrix}. \quad (56)$$

For positive bias $eV > 0$, the main process contributing to phonon emission is the inelastic electronic transition from the filled, left scattering states ψ_L to the empty, right states ψ_R . The transition rate is proportional to the modulus square of the matrix element,

$$|M_{LR}^q|^2 = |M_{RL}^{-q}|^2 \sim \cos^2 \frac{1}{2}(q - k_L + k_R). \quad (57)$$

The emission probability of a right-travelling phonon mode q ($q > 0$) is different from that of a left-travelling mode, $-q$. The difference is

$$\Delta M_{LR} = |M_{LR}^q|^2 - |M_{LR}^{-q}|^2 \sim \sin(q) \sin(k_L - k_R), \quad (58)$$

and as a result, the left and right-travelling steady state phonon populations becomes different. The difference changes sign upon changing the current direction which reveal the importance of electron momentum.

Next, we use the retarded phonon Green's function to consider the response, $|r\rangle$, of the phonon system to the asymmetric excitation, $|s\rangle \sim (\cdots 0 \ 1 \ e^{iq} \ 0 \ \cdots)^T$, at n and $n+1$, and find

$$|\langle m|r\rangle|^2 \sim |\langle m|D_0^r|s\rangle|^2 \sim \begin{cases} \cos^2 \frac{q+|q|}{2}, & m \ll n \\ \cos^2 \frac{q-|q|}{2}, & m \gg n \end{cases} \quad (59)$$

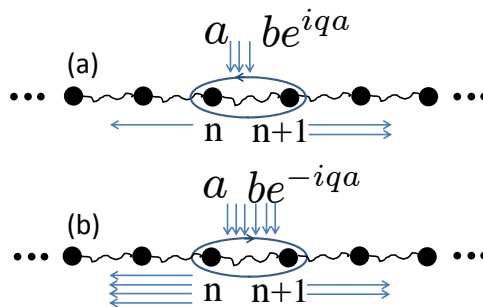


FIG. 4: The motion of atom n and $n + 1$ has a phase shift of $\pm q$. Within the configuration space of u_n and u_{n+1} , the two situations correspond to elliptical motion in opposite directions. The excitation probabilities of these two modes differs. This results in (1) an asymmetric heat flow to the left and right phonon bath, (2) polarization of the motion within configuration space (u_n, u_{n+1}) .

where obviously the response differs at the left and right side of the perturbation (Fig. 4).

We conclude that the applied bias breaks the population balance between left and right electron scattering states. Consequently, electrons excite the left and right travelling phonon states differently resulting in transfer of both energy and momentum to the phonons. The momentum transfer generates a different phonon energy flux to the left and right for the spatially symmetric system under bias. A schematic diagram of these processes are shown in Fig. 4. If we turn on the e-ph interaction at all the sites, the interaction matrix becomes $M_{LR}^q \sim \delta(k_L - k_R - q - 2N\pi)$. The asymmetric phonon excitation reduces to the rule of crystal momentum conservation in the periodic structure.

To make connection with the current-induced NC and BP force, in Fig. 4 we illustrate the orbital of the two phonon excitation within the configuration space of (u_n, u_{n+1}) . They are elliptical and related by time-reversal. From this point of view, the current-induced NC and BP forces polarize the atomic orbital motion, and generate a net angular momentum. The heat flow into the two electrodes becomes different due to this elliptical polarization.

Finally, it is instructive to compare the scattering analysis against the Langevin approach. In fact, one can show that

$$\text{Im}\langle\psi_L|M^n|\psi_R\rangle\langle\psi_R|M^{n+1}|\psi_L\rangle \sim \sin(k_L - k_R), \quad (60)$$

and

$$(\text{Im}\tilde{\mathcal{A}}_L^0)_{n+1,n}(\omega_q) \sim \sin(q). \quad (61)$$

So, comparing Eqs. (35) and (58), we can see that the asymmetric heat flow can indeed be understood as a result of asymmetric excitation of left- and right-travelling phonon waves.

V. SUPPORTING FIGURES FROM THE FIRST-PRINCIPLES CALCULATION

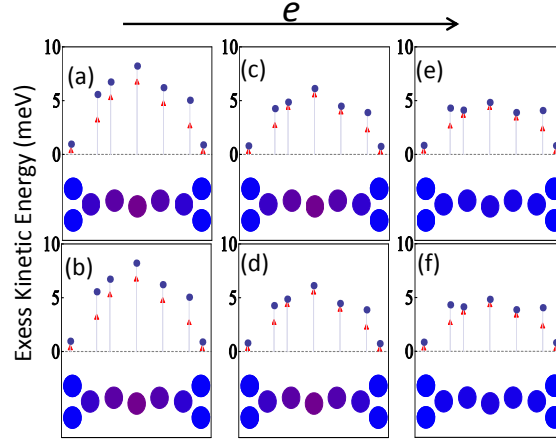


FIG. 5: Excess kinetic energy averaged over atoms in each column at $V = 1.0$ V, $T = 300$ K, similar to Fig. 2 in the main text. The top part (a), (c), (e) shows results without the asymmetric current-induced forces, while the bottom part (b), (d), (f) shows results that include only the BP and asymmetric fluctuating force. This shows the contribution from the BP and fluctuating force is negligible.

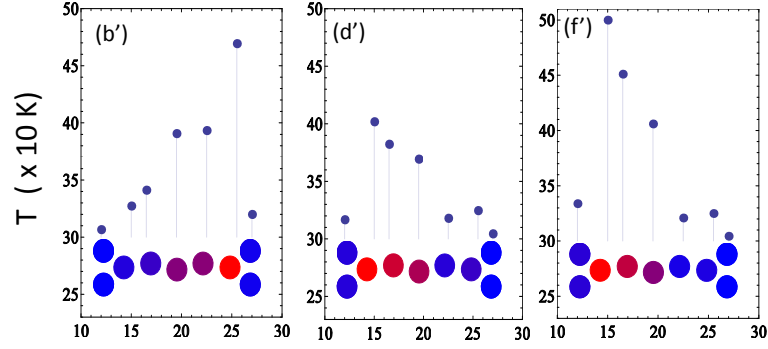


FIG. 6: Another way of characterizing heating in the chain is to use the Büttiker probe (Refs. [40-44] of the main text) to ‘measure’ the temperature of each atom. (b’), (d’) and (f’) show the ‘measured’ temperature of each atom using this method when including all the forces. The overall heating profile agrees with Fig. 2(b), (d), (f) in the main text.

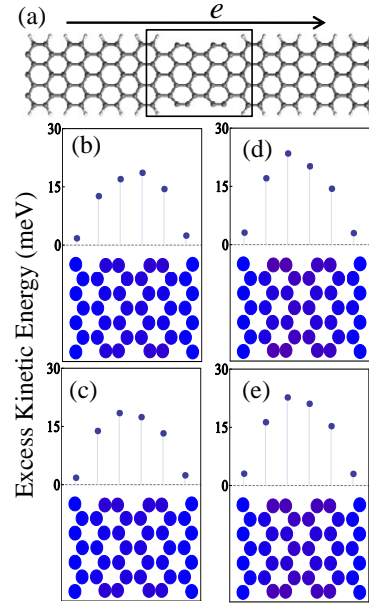


FIG. 7: Excess kinetic energy averaged over atoms in each column at $V = 0.4$ V, $T = 300$ K, similar to Fig. 3 in the main text. The top rows are results without the asymmetric current-induced forces, while the results in the bottom row include the BP and asymmetric fluctuating force. Again, their contribution to the asymmetric heating is negligible.

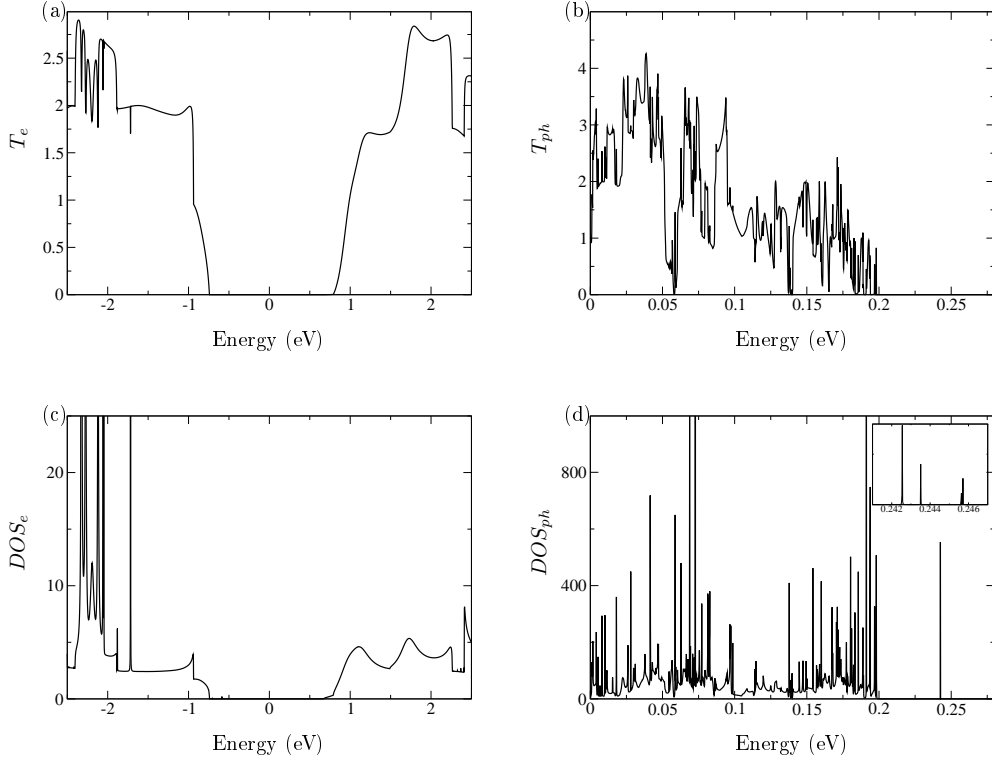


FIG. 8: Additional information on the Graphene nanoribbon calculation. (a) Electronic transmission (T_e). (b) Phononic transmission (T_{ph}). (c) Electronic density of states (DOS_e) projected to the device region. (d) Phononic density of states (DOS_{ph}) projected to the device region. In the SIESTA/TRANSIESTA DFT-calculation the following settings was used. Exchange-correlation functional: GGA-PBE. Basis-set: Single zeta polarized. Real space mesh cutoff: 400 Rydberg. The structure was relaxed until the forces on the atoms in the device region was below 0.01 eV/Ang.